RSC Advances

ROYAL SOCIETY OF CHEMISTRY

www.rsc.org/advances

Spraydrying as a novel and scalable fabrication method for nanostructured CsH_2PO_4, Pt-thin-film composite electrodes for solid acid fuel cells

R. C. Suryaprakash,[a,b] F. P. Lohmann[a], M. Wagner[a], B. Abel[a] and A. Varga[a]

ABSTRACT

Spraydrying was explored as a new CsH_2PO_4 nanoparticle synthesis method and a systematic parameter study was conducted to discover the set leading to optimal deposition rate and particle size distribution for applications in solid acid fuel cell electrodes. The nanoparticles were deposited directly onto either carbon paper current collector or a dense CsH_2PO_4 electrolyte pellet with a deposition rate of 1 mg h^{-1} cm^{-2} measured to be the same order of magnitude as previously employed electrospray. However, the total nanoparticle production rate is with 165 mg/h almost two orders of magnitude higher than the total production rate of electrospray. Novel, high performance solid acid fuel cell electrodes were fabricated by depositing CsH_2PO_4 nanoparticles onto a dense, uniaxially pressed CsH_2PO_4 electrolyte pellet, forming a three dimensional, porous, interconnected nanostructure, and thus providing a large surface area for subsequent Pt thin film deposition via magnetron sputtering. Electrochemical measurements *via* impedance spectroscopy in a symmetric cell configuration $Pt+CsH_2PO_4|CsH_2PO_4|CsH_2PO_4+Pt$ shows good reproducibility, excellent mass normalized activity as well as stability over a 24 h period.

GRAPHICAL ABSTRACT

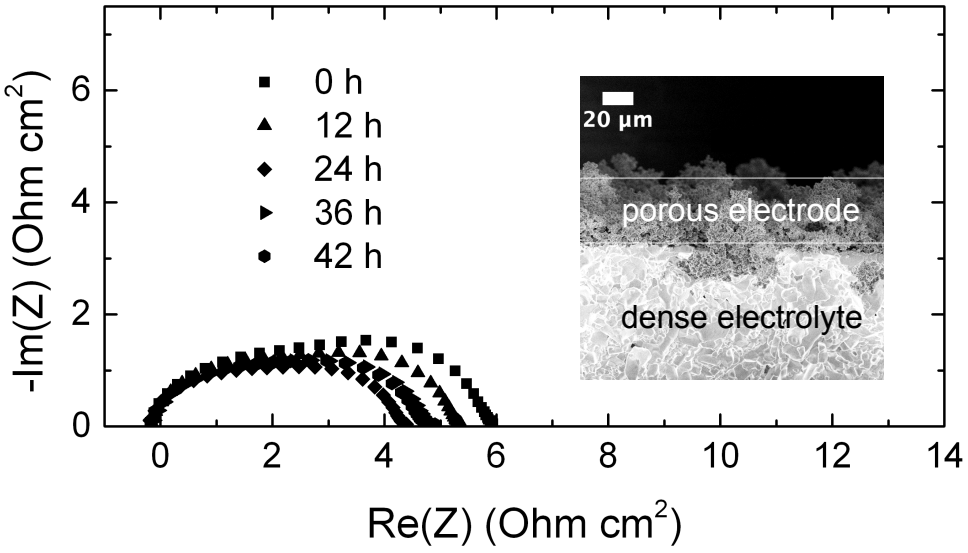

Journal Name

RSCPublishing

ARTICLE

Spraydrying as a novel and scalable fabrication method for nanostructured CsH_2PO_4, Pt-thin-film composite electrodes for solid acid fuel cells

Cite this: DOI: 10.1039/xoxxoooooox

Received ooth January 2012,
Accepted ooth January 2012

DOI: 10.1039/xoxxoooooox

www.rsc.org/

R. C. Suryaprakash,[a,b] F. P. Lohmann[a], M. Wagner[a], B. Abel[a] and A. Varga[a]

Spraydrying was explored as a new CsH_2PO_4 nanoparticle synthesis method and a systematic parameter study was conducted to discover the set leading to optimal deposition rate and particle size distribution for applications in solid acid fuel cell electrodes. The nanoparticles were deposited directly onto either carbon paper current collector or a dense CsH_2PO_4 electrolyte pellet with a deposition rate of 1 mg h^{-1} cm^{-2} measured to be the same order of magnitude as previously employed electrospray. However, the total nanoparticle production rate is with 165 mg/h almost two orders of magnitude higher than the total production rate of electrospray. Novel, high performance solid acid fuel cell electrodes were fabricated by depositing CsH_2PO_4 nanoparticles onto a dense, uniaxially pressed CsH_2PO_4 electrolyte pellet, forming a three dimensional, porous, interconnected nanostructure, and thus providing a large surface area for subsequent Pt thin film deposition via magnetron sputtering. Electrochemical measurements *via* impedance spectroscopy in a symmetric cell configuration $Pt+CsH_2PO_4|CsH_2PO_4|CsH_2PO_4+Pt$ shows good reproducibility, excellent mass normalized activity as well as stability over a 24 h period.

1. Introduction

As an increasing proportion of the energy supply is generated with variable and intermittent photovoltaic and wind power, efficient energy storage technologies are becoming necessary. Chemical energy systems have been identified as a suitable form of grid scale energy storage, therefore highly efficient energy conversion devices are needed from electrical to chemical form and vice versa. Fuel cells have attracted much attention in the past because of their high conversion efficiency, but their widespread application is hindered by high material and fabrication costs.

Solid acid fuel cells (SAFCs) represent a promising and relatively new technology, providing multiple distinct advantages over other technologies.[1] The intermediate operating temperature of 240°C, together with the solid-state electrolyte allows easy handling and fuel flexibility.[2] A 415 mW/cm^2 performance was recently demonstrated by Uda et. al. with a platinum loading of 7.7 mg/cm^2. Unpublished results by SAFCell inc. Pasadena show a slight increase in power density with a ca. 3 mg/cm^2 Pt loading.[3, 4] However, widespread application is still hindered by the high platinum catalyst loading of the composite electrodes.[5] Significant efforts have been made towards lowering the platinum loading, mainly by decreasing the electrolyte feature size and improving the electrical connectivity of catalyst nanoparticles.[4, 6] Specifically, electrospray deposition has been shown to effectively produce electrolyte particles with down to 100 nm diameter. Deposition of the nanoparticles results in interconnected, 3-dimensional nanostructures with well dispersed, co-deposited Pt, Pt on C catalyst nanoparticles, as well as the stabilizing polymer polyvinylpyrrolidone (PVP). Despite these successes in the laboratory, large scale employment of this technology is hindered by the low throughput and deposition rate of only ca. ~1.8 mg h^{-1} cm^{-2}.[6] For practical applicability, a deposition rate of an order of magnitude higher, on substrates of 7.5 cm diameter (SAFCell inc. Pasadena, prototype) is regarded to be necessary.

Furthermore, recent studies on the fundamental reaction mechanisms at solid acid fuel cell anodes have revealed a significantly higher mass normalized activity of the platinum catalyst in the form of thin films compared to nanoparticles. For sputter-deposited continuous films, thinner than 50 nm, the hydrogen diffusion rate is sufficiently fast so that the interfacial process at the Pt-electrolyte interface is rate limiting. Thus the

two-phase boundary pathway is dominant over the classical three-phase boundary pathway. The maximum mass normalized electrode activity of 19 S/mg was measured with 8 nm thin Pt-films, which is an almost 9-fold increase compared to previous composite electrodes employing Pt nanoparticles (2.2 S/mg).[7] These findings reveal the ideal solid acid fuel cell anode to be a porous electrolyte nanostructure uniformly covered with a platinum thin film. Such electrodes have the potential to lower the Pt loading by an order of magnitude while reaching state of the art electrode performance.[7]

As the first step towards fabricating such electrodes, we explore spraydrying, using a commercial system. The spraydrying method has the potential to overcome the low deposition rate of previously employed electrospray system while maintaining a similarly small electrolyte feature size. Spraydrying has been widely utilized to synthesize nano- and microparticles of polymers, ceramics, food and medical compounds in the nanometer size-range and a production rate of 100s of mg/h.[8-11]

The aim of this work is to establish spraydrying as a scalable method to deposit CsH_2PO_4 solid acid electrolyte nanoparticles and to create porous, 3-dimensional interconnected nanostructures of the solid acid fuel cell electrolyte material CsH_2PO_4. Furthermore, we wish to demonstrate their functionality as solid acid fuel cell anodes with subsequent deposition of a platinum thin film.

2. Experimental

2.1 Materials

The solid acid electrolyte material CsH_2PO_4 was synthesized *via* a new route compared to previously reported method.[12] Cs_2CO_3 (99.9% purity, Alfa Aesar, Stk# 10928) was dissolved directly in methanol rather than deionized water and added to a stoichiometric quantity of H_3PO_4 (85vol%, Alfa Aesar, Stk# A18067) mixed with methanol while stirring and allowed to react to CsH_2PO_4 according to equation (1).

$$Cs_2CO_{3(MeOH)} + H_3PO_4 \text{ --> } CsH_2PO_{4(s)} + CO_{2(g)} + H_2O \qquad (1)$$

Solid CsH_2PO_4 particles precipitate rapidly, as the reaction product has negligible solubility in methanol. The precipitate was filtered from the suspension and dried overnight at 80°C in a drying oven. The synthesis was confirmed with X-ray powder diffraction.

For spraydrying, the electrolyte material CsH_2PO_4 was re-dissolved (0.1 – 10 g/L) in methanol-water mixtures (0 – 66 wt% methanol). For selected solutions, the polymer polyvinylpyrrolidone (PVP, Sigma Aldrich, M_w 10,000, Stk# PVPV10-100G; Alfa Aesar, M_w 1,300,000, Stk# 43728) was added (0.1 – 10 g/L) as a means to stabilize the deposited nanostructure. As the deposition substrate, Teflon treated or Teflon free carbon paper (Toray TGP-H-060) or uniaxially pressed CsH_2PO_4 pellets were used. A microprocessor controlled uniaxial press (Atlas Auto T15 programmable press) was used to fabricate the CsH_2PO_4 pellets (2 cm dia., 0.5 mm thickness) from the dry, sieved powder (75 μm final mesh size), resulting in 98% density. Since the employed substrates also serve as fuel cell components (current collector or electrolyte layer), no post synthesis particle processing was necessary. Selected PVP-containing samples were plasma treated using a pure oxygen DC plasma (Diener electronic Femto plasma system) for removal of PVP. We employed a pure oxygen DC-plasma with the sample placed in the plasma generation area for various times (5, 15, 30 min). The plasma power was set to 100 W and the oxygen flow rate to 10 sccm.

For three CsH_2PO_4 pellets, spraydeposition of a CsH_2PO_4 nanostructure was completed on both sides of the electrolyte pellet and a 10 nm thin platinum film was deposited via sputtering (Edwards Magnetron Sputterer Auto 306) creating a symmetric cell $Pt+CsH_2PO_4 \mid CsH_2PO_4 \mid CsH_2PO_4+Pt$ for subsequent electrochemical characterization. The sputterer is equipped with a thickness monitor to control deposited film thickness.

2.2 Spraydrying

The commercial spraydryer Büchi® Nanospraydryer B-90 (Büchi Labortechnik AG, Flawil, Switzerland) was used in all nanoparticle synthesis experiments, Fig. 1.

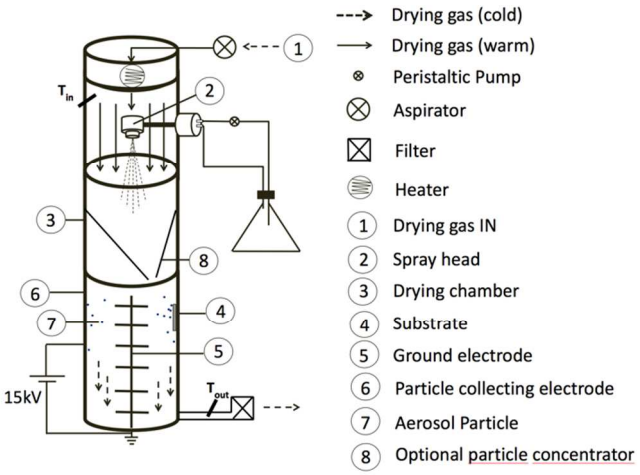

Fig. 1 Schematic of Büchi B-90 Nanospraydryer (after www.büchi.com)

In brief, the precursor solution is circulated uniformly from a reservoir with a variable speed peristaltic pump through the spray head back to the reservoir. The spray head consists of a small chamber with a stainless steel mesh at the base. The mesh is brought to oscillation with piezoelectric transducers, so that micrometer sized droplets are ejected into the drying chamber. Three different meshes were employed with varying hole sizes of 4, 5.5, and 7μm. The aerosol droplets are transported in the drying chamber with a dry carrier gas (linear velocity 144 - 361 cm/min) consisting of nitrogen and carbon dioxide towards an electrophoretic deposition area. Carbon dioxide prevents dielectric breakdown at the deposition electrode. During droplet flight, the solvent evaporates and CsH_2PO_4 precipitates, forming dry solid particles. In the deposition area, an outer cylinder is held at a high voltage relative a stack of star-shaped, grounded center electrodes. A glow discharge at the star-tips of the center electrodes ionizes the drying gas. The solid aerosol particles become charged through collisions and are deflected towards an outer, grounded metal cylinder. For an increased deposition rate on a specific area, a concentring semi-porous, cardboard funnel was employed in the drying chamber just before the deposition area. The aerosol was deposited on carbon paper (2x2 cm) and CsH_2PO_4 pellets attached to the cylinder with doubles-sided conducting carbon tape. The drying gas was filtered and re-circulated via the Inert Loop B-295

system, in a closed-mode setting. The oxygen concentration of the drying chamber was kept below 4%.

2.3 Characterization

The as-synthesized CsH_2PO_4 powder and as-deposited CsH_2PO_4 particles were characterized by X-ray powder diffraction (Rigaku, Ultima IV, Cu-Kα radiation, λ = 0.15418 nm, V = 40 kV, I = 40 mA, 2θ range of 20 to 60°).

The surface tension of precursor solutions with varying methanol concentration was determined with the DuNuoy ring method (Sigma 703 tensiometer), using a platinum ring.

The deposited particle size distribution on the carbon paper substrates and the morphology of the nanostructures as well as the sputtered Pt film was determined and characterized using scanning electron microscopy equipped with an EDX detector (ZEISS 1550VP Field Emission SEM, Bruker EDX XFlash 3001). The particle sizing and size distribution statistics were conducted with image processing software ImageJ v.1.48.

The removal of polymer with oxygen plasma treatment was confirmed with infrared spectroscopy (Bruker Vector 2, 4000 – 400 cm^{-1}).

The electrochemical performance of spraydryer-deposited, nanostructured CsH_2PO_4 and platinum thin film electrodes was characterized with AC impedance spectroscopy (Eco Chemie Autolab PGSTAT302 and Biologic VSP 300) at 240ºC in a humidified hydrogen atmosphere. The measurements were conducted in a symmetric cell configuration at 240°C in humidified hydrogen (pH_2O = 0.4 atm), in a frequency range of 100 mHz to 1 MHz. A control experiment with a polished CsH_2PO_4 pellet and 20 nm sputtered Pt thin film electrodes was conducted to compare with results of Louie et. al.[7]

3. Results and Discussion

Nanoparticle Synthesis

The compositional purity of the as synthesized CsH_2PO_4 powder and the spraydryer deposited powder was confirmed with powder X-ray diffraction, Fig. 2.[13]

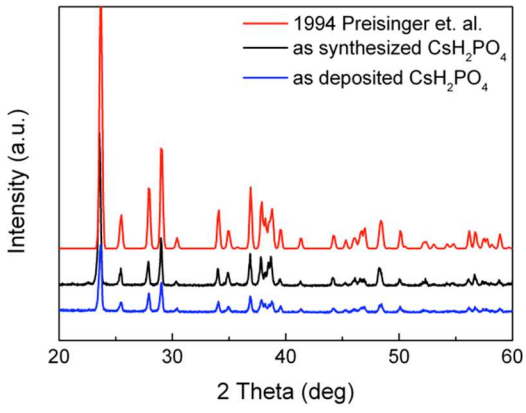

Fig. 2 X-ray diffraction pattern of as synthesized and as deposited CsH_2PO_4 and corresponding reference pattern.[13]

Representative SEM micrographs of CsH_2PO_4 nanoparticles obtained with the nanospraydryer and directly deposited on carbon paper are shown in Fig. 2. The carbon paper substrates were positioned along a line at various heights of the particle-collecting electrode in order to observe variations of the deposition rate and particle size distribution at the default spraying parameter set, Fig. 3.

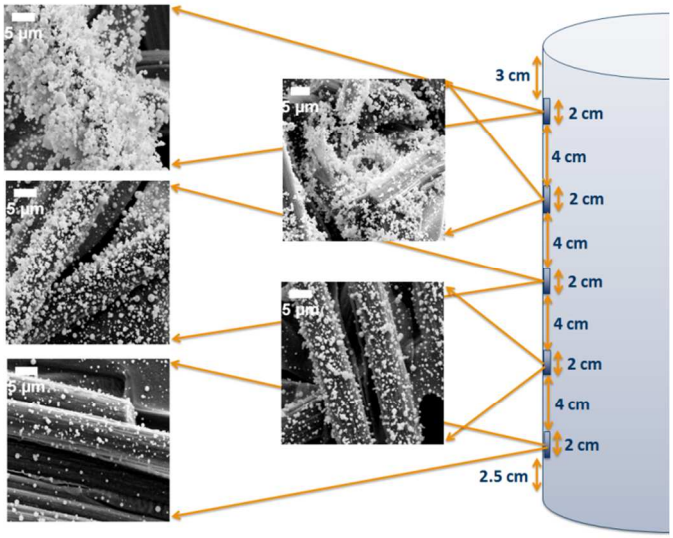

Fig. 3 Scanning electron micrographs of CsH_2PO_4 particles deposited via spraydrying onto carbon paper at various positions of the particle-collecting electrode.

The deposition rate decreases monotonically downstream of the particle collecting electrode from 0.5 mg h^{-1} cm^{-2}, to <0.1 mg h^{-1} cm^2. Both values are much smaller than the total particle generation rate of 165 mg/h, as calculated from the spraying rate. A significant increase in the deposition rate up to 1 mg h^{-1} cm^{-2} was obtained at the topmost position by covering a 5 x 5 cm^2 area around the carbon paper deposition substrate with insulating tape, thus effectively increasing the local electric field strength at the carbon paper, driving more particles towards it. More importantly a 2 mg h^{-1} cm^{-2} deposition rate was obtained by employing a funnel-shaped particle concentrator, Fig. 4. Even though the deposition efficiency is only 2%, the deposition rate is of the same order of magnitude as with electrospray deposition. There is great potential for much increased deposition rate and area with an optimized particle collector. This result is very significant, as the widespread application of nanoparticles for solid acid fuel cells electrodes has been hindered mainly by the low synthesis rate.

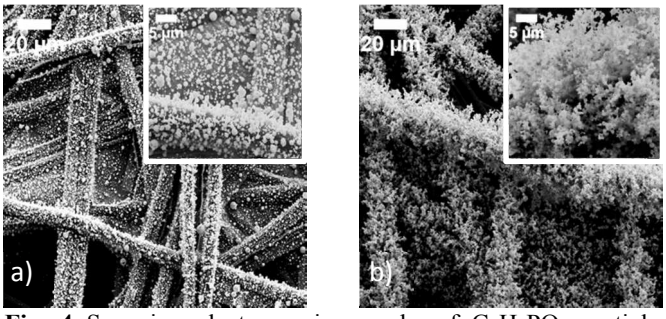

Fig. 4 Scanning electron micrographs of CsH_2PO_4 particles spraydryer deposited for 120 min on carbon paper (a) without particle concentrator and (b) with particle concentrator. Higher magnification is shown in inset.

To further optimize the deposition rate and the particle size distribution, a parameter study was conducted, varying both spray parameters and precursor solution parameters, Table 1.

Table 1 Spraydryer and precursor solution parameters ranges employed for the optimization of the deposition, with default indicated.

Parameter	Range	Default
CsH_2PO_4 concentration (g/L)	0.1 - 10	1
Methanol concentration (wt %)	0 - 66	44
Polyvinylpyrrolidone concentration (g/L)	0 - 10	0
Temperature (°C)	30 - 120	30
Carrier gas flow rate (L/min)	60 - 150	70
Pump rate (ml/min)	1.5, 7, 16.5, 17	1.5
Mesh size (µm)	4, 5.5, 7	4

To exclude the chance of particle agglomeration, samples with very light particle loading was utilized where the nanoparticles remained spatially separated. Representative particle size distributions obtained from analysis of SEM images are shown in Fig. 5a for six different CsH_2PO_4 concentrations ranging from 0.1 to 10 mg/L. The distributions were fitted with a log-normal function, which is the typical size distribution for aerosolized particles.[14] The corresponding mean particle diameter and standard deviation (plotted as bars) is shown in Fig. 5b. The same procedure was used for all other parameters sets. The mean diameter of the particles increases monotonically with increasing CsH_2PO_4 concentration A cube-root function is an excellent fit to the data, indicating that the initial droplet size does not vary significantly with the CsH_2PO_4 concentration. Assuming there is no significant particle agglomeration, the initial droplet diameter can be calculated from the final particle diameter and the solution concentration. The calculated values range from 3.0 to 4.7 µm, which is in line with the expected value for a 4 µm spray mesh size.[15] Thus the increase in the final mean particle diameter from 150 nm to 540 nm mainly stems from the increase in the solute concentration.

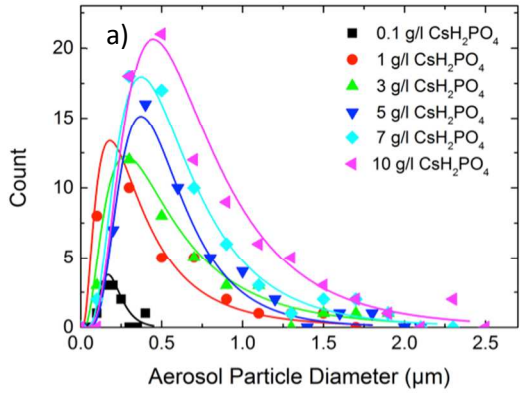

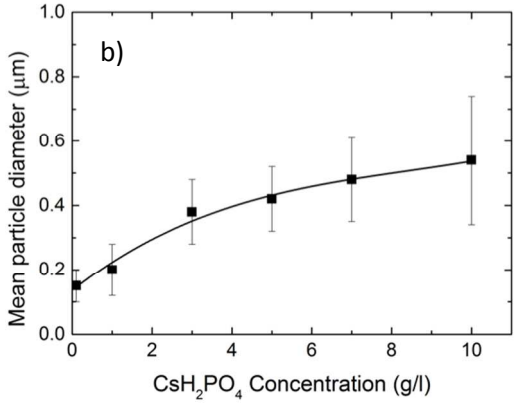

Fig. 5 a) CsH_2PO_4 particle size distribution for different precursor solutions with varying CsH_2PO_4 concentrations b) corresponding mean particle diameter from the log-normal fitting as a function of CsH_2PO_4 concentration in the precursor solution.

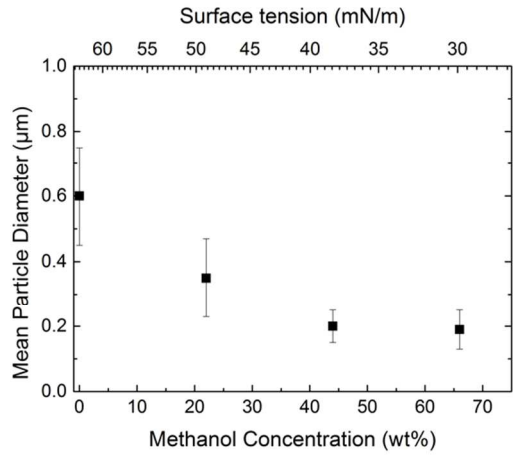

Fig. 6 Mean particle diameter as a function of methanol concentration of the precursor solution and corresponding surface tension.

The second precursor solution parameter examined was the methanol concentration of the solvent. With increasing methanol concentration, the surface tension decreases, resulting in smaller initial droplets. This in turn results in smaller particles, Fig. 6. Since CsH_2PO_4 solubility in methanol is negligible, the solubility limit decreases with increasing methanol concentration of the precursor solution. This boundary limits the deposition rate for higher methanol concentrations. Therefore 44 wt% methanol is proposed as the optimum concentration for the smallest particle size.

The polymer polyvinylpyrrolidone has been employed previously as a stabilizing component for the deposited CsH_2PO_4 nanostructure.[6] Here we take the same approach and co-deposit a solution of CsH_2PO_4 + PVP (10,000 M_w and 1,300,000 M_w). The monotonic increase of the final particle size, Fig. 7., can be simply explained by the increase in the PVP concentration per droplet. The initial droplet size remains in the expected range of 3.4 to 4.7 µm for the 4 µm spray mesh size.

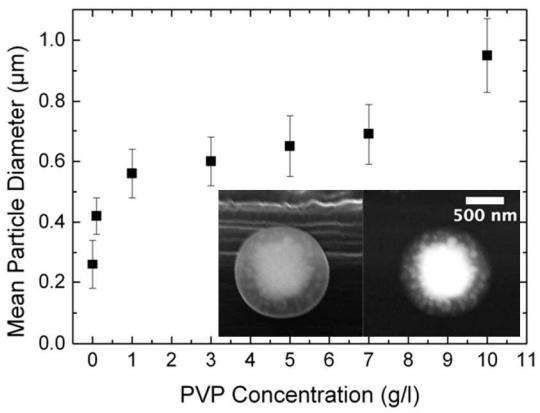

Fig. 7 Mean CsH_2PO_4 particle diameter as a function of PVP concentration in the precursor solution; Inset: scanning electron micrograph of deposited CsH_2PO_4 + PVP particles forming a core-shell structure taken with a secondary electron (left) and backscattered electron (right) detector.

The inset in Fig. 7 shows a representative separated particle from the deposition with 10 g/L PVP (M_w 1000) and 10 g/L CsH_2PO_4, with a core-shell structure imaged with a secondary (left) and backscattered (right) electron detector. The denser inner core is likely to be CsH_2PO_4 while the outer shell is PVP. Such core shell particles have not been observed with pure CsH_2PO_4 solutions. This observation sheds light on the open question of presence of the polymer after deposition. As reported previously[6], PVP (M_w 1,300,000) effectively stabilizes the deposited nanostructure at the fuel cell operating conditions, while pure CsH_2PO_4 particles readily agglomerate within a few minutes at ambient conditions. However, for the electrode performance, fully coated particles are expected to be detrimental due to the negligible conductivity of PVP. Here, PVP removal was achieved with a pure oxygen plasma, similar to our previous reports. The corresponding FTIR spectra are presented in Fig. 8. IR absorption bands are clearly visible for the untreated, as deposited sample at 1285 cm^{-1} (CH_2 wag.), 1430 cm^{-1} (CH_2 scissors) and 1650 cm^{-1} (carbonyl stretch) which are the characteristic absorption bands for PVP.[16] With increasing plasma treatment time, the absorption peak intensities decrease, and no PVP was detected after 30 min oxygen plasma exposure.

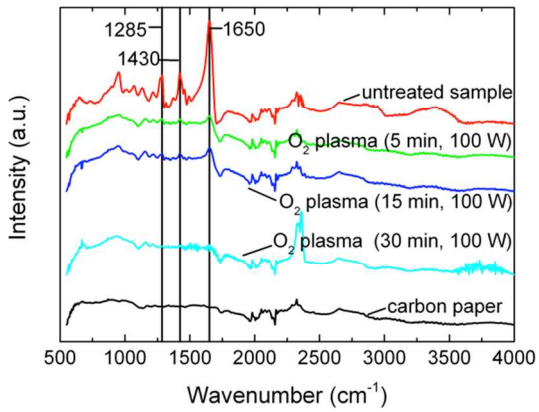

Fig. 8 FTIR spectra of (i) as deposited sample (CsH_2PO_4 + PVP), oxygen plasma treated sample after (ii) 5 min, (iii) 15 min, (iv) 30 min exposure time and (v) blank carbon paper substrate.

Turning to the process parameters, the dry carrier gas flow rate was varied between 60 and 150 L/min, corresponding to 144 and 360 cm/min linear flow velocities. Assuming laminar flow, the aerosol residence time in the drying chamber is between 30 and 12 sec. Since the evaporation rate of micron sized droplets is of the order of milliseconds, the carrier gas flow rate does not have a significant influence on the final particle size, Fig. 9.[17]

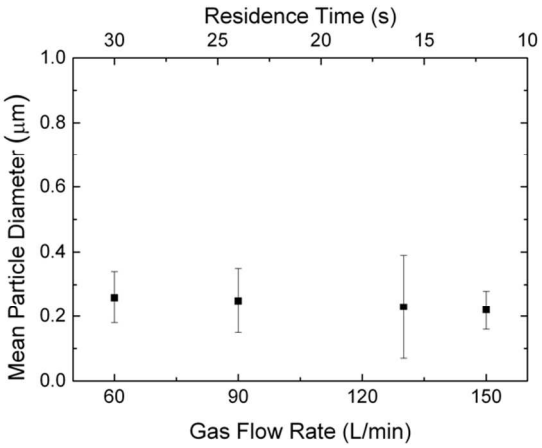

Fig. 9 Mean CsH_2PO_4 particle diameter as a function of dry carrier gas flow rate and corresponding residence time before deposition.

The dry carrier gas temperature was varied between 30°C and 120°C, as measured with a thermocouple at the top of the drying chamber. The carrier gas temperature decreases downstream due to heat loss from the evaporating solvent and through the chamber walls. The carrier gas temperature has no significant effect on the final CsH_2PO_4 particle size except for at very high temperatures. Interestingly, for T = 120°C, hollow-sphere particles are visible on scanning electron micrographs, Fig. 10 inset.

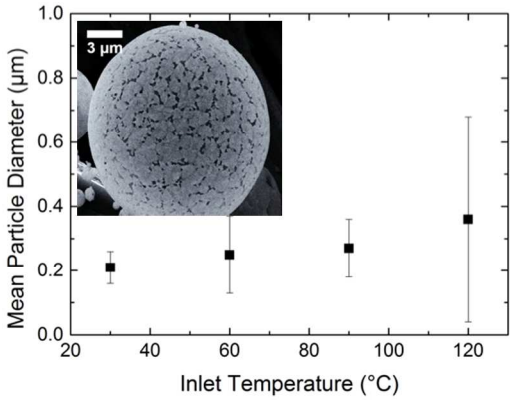

Fig. 10 Mean CsH_2PO_4 particle diameter as a function of carrier gas temperature at the top of the drying chamber. Inset: Scanning electron micrograph of a representative, hollow CsH_2PO_4 particle deposited at a temperature setpoint of 120°C.

When the evaporation rate of the solution is higher than the convection rate, a concentration gradient is established and the solute precipitates at the surface. This process has been observed and described previously by Charlesworth et. al. and Jayanthi et. al.[17, 18] For a uniform particle size distribution with solid CsH_2PO_4 nanoparticles, mild carrier gas temperature of 30°C is sufficient.

The spray mesh hole size has a significant influence on the mean CsH_2PO_4 particle size, Fig. 11. With increasing mesh hole size, we measure an increasing mean CsH_2PO_4 diameter. The calculated initial droplet size is 3, 4.4 and 7.4 µm respectively, which is in line with the expected values and explains the trend.

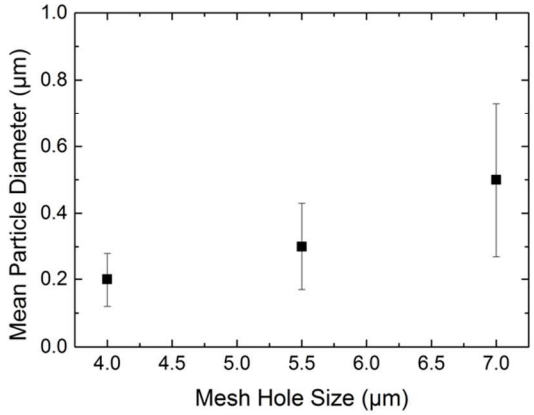

Fig. 11 Mean CsH_2PO_4 particle diameter as a function of mesh hole diameter of the spray head membrane.

The final process parameter varied was the precursor solution circulation rate (not actual spray rate). The mean CsH_2PO_4 particle size increases with the flow rate, Fig. 12. As the precursor solution is pumped over the porous membrane, the pressure inside the spray cap is thought to influence the initial droplet size but not the number concentration of the droplets.

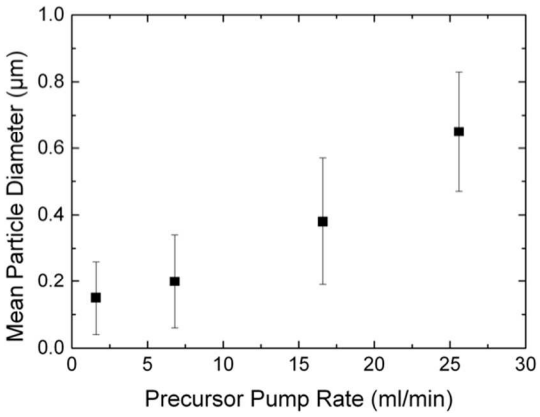

Fig. 12 Mean CsH_2PO_4 particle diameter as a function of precursor solution circulation rate (not spray rate) above the spray mesh.

Electrochemical measurements

Similar to the electrospray system in our previous reports, the spraydryer is capable of depositing CsH_2PO_4 nanoparticles onto a prepressed, pure CsH_2PO_4 pellet. Normally, electrophoretic deposition requires some electrical conductivity of the substrate in order to dissipate charge and to maintain a steady deposition rate. Charge dissipation here, is thought to occur via the gas phase, through collisions with neutral gas molecules as the CsH_2PO_4 pellet has negligible conductivity at room temperature.

Depositing for 1 hour onto a CsH_2PO_4 pellet with the default set of parameters results in a continuous 20 – 30 µm thick porous CsH_2PO_4 structure, Fig. 13.

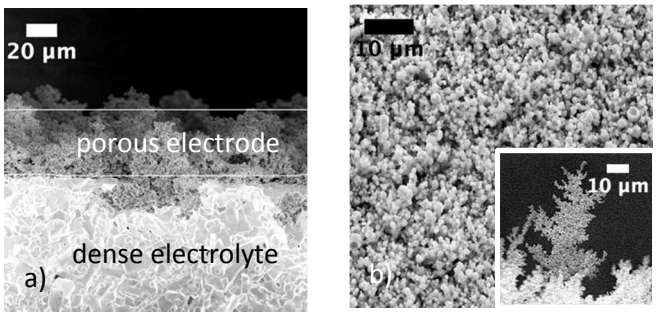

Fig. 13 a) Side view and b) Top view scanning electron micrographs of porous CsH_2PO_4 nanostructure on pressed CsH_2PO_4 pellet, obtained via spraydrying. The inset shows a scanning electron micrograph of a CsH_2PO_4 structure at the very edge of the electrolyte pellet.

For electrochemical measurements in a symmetric cell geometry, the CsH_2PO_4 nanostructured, porous layer was deposited on both sides of a uniaxially pressed CsH_2PO_4 electrolyte pellet (2 cm dia., 0.5 mm thickness). A nominally 10 nm thick platinum film -as determined by the thickness monitor- was sputtered onto both sides of the pellet. As sputtering is a line-of-sight-deposition technique, the exposed

features of the porous nanostructure are covered with the nominal Pt thickness whereas a thinner film or no coverage is expected deeper inside the pores due to shadowing effects. This is confirmed qualitatively in Fig. 14, showing an SEM micrograph of an electrode cross-section with false color representation of Pt coverage of the porous CsH_2PO_4 structre, obtained with EDX mapping.

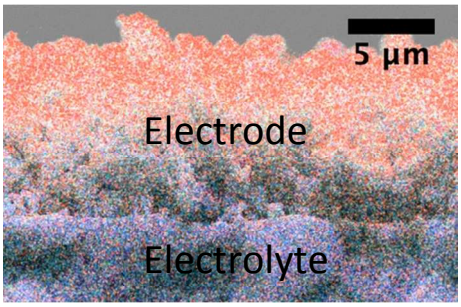

Fig. 14 SEM micrograph of an electrode cross-section with a false color representation of sputtered Pt (orange) thin-film obtained by an EDX detector, showing good Pt coverage at the top of the structure and negligible near the electrolyte (Cs in blue) interface.

The Pt loading of the cell is calculated from the geometry of the nominal Pt coverage (area x nominal thickness x density) to be 0.021 ± 0.002 mg/cm^2. The experimental error stems from the error of the thickness monitor of the sputterer.

Fig. 15 shows electrochemical impedance results in the Nyquist representation, for two separate Pt-film+CsH_2PO_4|CsH_2PO_4|CsH_2PO_4+Pt-film cells measured in humidified hydrogen atmosphere at 240°C, with the electrolyte response subtracted. The polymer PVP with 58,000 molecular weight is employed here. The initial electrode performance for the two separate electrodes shows good reproducibility as well as remarkable mass normalized activity of 13 S/mg. This is more than a 5-fold increase compared to the best electrosprayed CsH_2PO_4+Pt nanoparticles previously reported.[6] However, the initial good performance is followed by quick increase of the electrode impedance over a 12 and 24 h period. The degradation process can be explained by the thermal instability of PVP-M_w58,000 at the fuel cell operating conditions and the agglomeration of the porous CsH_2PO_4 nanostructure. This hypothesis is supported by the much improved stability of similarly fabricated symmetric cells but with PVP-M_w 1,300,000 employed as compared to identically fabricated electrodes but with PVP-M_w58,000. Fig. 16 shows impedance spectra for a symmetric cell with good stability over a 42 h period at 240°C, in a humidified hydrogen environment (pH_2O = 0.4 atm). The initial performance improvement can be attributed to improved contact between the electrolyte particles due to mild sintering. The mass normalized activity for this cell is 11.3 S/mg, which is a remarkable 5-fold increase compared to the best electrodes achieved via electrospray deposition. The control electrochemical experiment of a symmetric cell consisting of 10 nm thick Pt film electrodes on a polished CsH_2PO_4 pellet yielded a 3.6 Ω cm^2 electrode impedance and a mass normalized activity of 13.2 S/mg, Figure 16 inset. This is in line with the results of Louie et. al.[7] but shows that further improvements of the porous electrode performance are possible.

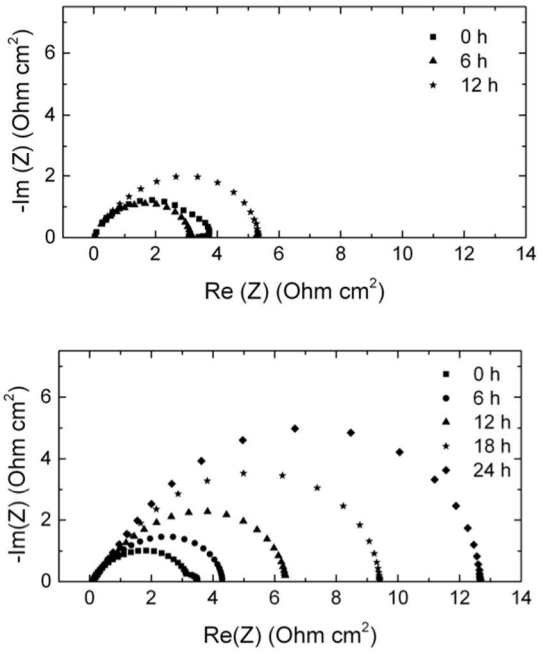

Fig. 15 a) and **b)** Impedance spectra of two Pt-thin-film – nanostructured CsH_2PO_4 electrodes with PVP-M_w58,000 taken over a 12 and 24 h period respectively at 240°C, H_2 atmosphere (pH_2O = 0.4 atm) and 0 V bias.

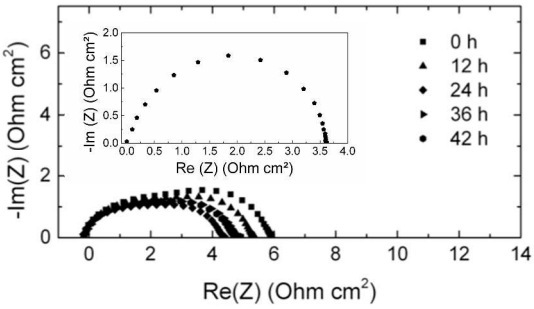

Fig 16. Impedance spectra of a symmetric cell electrode, consisting of 10 nm Pt-thin-film – nanostructured CsH_2PO_4 with PVP-M_w1,300,000, taken over a 42h period at 240°C, H_2 atmosphere (pH_2O = 0.4 atm), showing good stability after initial improvement. **Inset:** Control experiment with 10 nm Pt thin film sputtered onto a polished CsH_2PO_4 electrolyte pellet.

Conclusions

The results demonstrate that spraydrying is a promising new synthesis method for CsH_2PO_4 nanoparticles with the important, and technologically relevant advantage of higher possible throughput of 165 mg/h compared to 1.8 mg/h with

previously employed electrosprayed method and easier scalability. This overcomes a significant obstacle for the technological application of nanoparticle synthesis.

Platinum thin films on flat CsH_2PO_4 pellets have been demonstrated by Louie and Haile as a promising way to increase the mass normalized activity of platinum in solid acid fuel cell anodes as compared to platinum nanoparticles as two-phase boundary pathway is active in addition to the triple phase boundary.[7] Here we deposited a platinum thin film on a high surface area CsH_2PO_4 structure, combining high mass normalized activity and high surface area, resulting in significantly improved and stable hydrogen electrode performance. The platinum loading is 0.021 ± 0.002 mg/cm^2. The mass normalized activity of 11.3 S/mg for Pt represents a 5-fold increase towards the current state of the art for nanoporous electrodes and clearly demonstrates the potential for further enhancement with optimized nanoporous electrode and catalyst thin film thickness. A systematic study with varying catalyst thin film thickness and porous electrolyte layer thickness is necessary to determine the optimal electrode structure.

Acknowledgements

The authors are indebted to Prof. Sossina M. Haile for continuing, useful discussions. The authors acknowledge funding through the ESF-Forschergruppe "Applied and theoretical molecular electrochemistry as a key for new technologies in the area of energy conversion and storage". The authors are indebted to D. Hirsch and A. Sobottka for SEM and XRD measurements, respectively.

Notes and references

[a] Leibniz Institute of Surface Modification, Permoserstr. 15, D-04318 Leipzig, Germany.

[b] Hochschule Bremen, Neustadtswall 30, D-28199 Bremen, Germany.

1. S. M. Haile, C. R. I. Chisholm, K. Sasaki, D. A. Boysen and T. Uda, *Faraday Discussions*, 2007, 134, 17.
2. T. Uda, D. A. Boysen, C. R. I. Chisholm and S. M. Haile, *Electrochemical and Solid-State Letters*, 2006, 9, A261.
3. T. Uda and S. M. Haile, *Electrochemical and Solid-State Letters*, 2005, 8, A245-A246.
4. A. Varga, M. Pfohl, N. A. Brunelli, M. Schreier, K. P. Giapis and S. M. Haile, *Physical chemistry chemical physics : PCCP*, 2013, 15, 15470-15476.
5. C. Chisholm, D. A. Boysen, A. B. Papandrew, S. K. Zecevic, S. Cha, K. A. Sasaki, Á. Varga, K. P. Giapis and S. M. Haile, *Interface Magazine*, 1009, 3, 53-59.
6. Á. Varga, N. A. Brunelli, M. W. Louie, K. P. Giapis and S. M. Haile, *Journal of Materials Chemistry*, 2010, 20, 6309.
7. M. W. Louie and S. M. Haile, *Energy & Environmental Science*, 2011, 4, 4230.
8. X. Li, N. Anton, C. Arpagaus, F. Belleteix and T. F. Vandamme, *Journal of controlled release : official journal of the Controlled Release Society*, 2010, 147, 304-310.
9. S. H. Lee, D. Heng, W. K. Ng, H. K. Chan and R. B. Tan, *International journal of pharmaceutics*, 2011, 403, 192-200.
10. F. Gao, Z. Tang and J. Xue, *Electrochimica Acta*, 2007, 53, 1939-1944.
11. F. Wu, X. Li, Z. Wang, H. Guo, Z. He, Q. Zhang, X. Xiong and P. Yue, *Journal of Power Sources*, 2012, 202, 374-379.
12. M. W. Louie, K. Sasaki and S. M. Haile, *Electrochemical Society Transactions*, 2008, 13, 57-62.
13. A. Preisinger, K. Mereiter and W. Bronowska, *Proceedings of the third European Powder Diffraction Conference*, 1994, 166, 511-516.
14. M. R. Stolzenburg and P. H. McMurry, *Aerosol Science and Technology*, 2008, 42, 421-432.
15. Büchi, *Operational Manual Nano Spray Dryer B-90*, Flawil, Switzerland, 2009.
16. Y. Borodko, H. S. Lee, S. H. Joo, Y. Zhang and G. Somorjai, *Journal of Physical Chemistry C*, 2011, 115, 4757-4767.
17. G. V. Jayanthi, S. C. Zhang and G. L. Messing, *Aerosol Science and Technology*, 1993, 19, 478-490.
18. D. H. Charlesworth and W. R. Marshall Jr., *AIChE Journal*, 1957, 6, 9-23.

